HYDRAULIC PROPERTIES AND ENERGY DISSIPATION OF DEEP HARD ROCK UNDER H-M COUPLING AND CYCLING LOADS

by

Cheng-Han ZHANG, Shuang YOU*, Hong-Guang JI, Fei LI, and Hong-Tao WANG

School of Civil and Resource Engineering,
University of Science and Technology Beijing, Beijing, China

Original scientific paper
https://doi.org/10.2298/TSCI180702181Z

The permeability of deep rock is closely related to the stability and safety of underground engineering. The rocks in deep stratum are mostly with high stress and high osmotic pressure. Therefore, it is necessary to consider the coupling effect between porewater pressure and in situ stress on rock mass. A series of triaxial cyclic loading and unloading experiments under hydraulic-mechanics coupling conditions are carried out to studied the mechanical and hydraulic properties of granite in the depth of 1300 m to 1500 m. Especially, the effect of the disturbance on the permeability of fractured rocks are investigated by unloaded the confining pressure. Tests results presented that the stress-strain curves of deep granite showed typical brittle characteristics. The principal stress of granite exhibited a linear relationship under the high confining pressure of 34-40 MPa and high osmotic pressure of 13-15 MPa. Dissipated energy of the rock decreased to a relatively low level after 2-3 loading cycles and then slowly increased. Permeability showed a decreasing trend as the loading and unloading cycles increase. Finally, acoustic emission technology was used to monitor the fracture evolution in rocks, the acoustic emission signal released as the fractures develop and energy dissipated. The results would provide basic data for the exploitation and excavation in the deep galleries.

Key words: *deep stratum, granite, hydraulic-mechanics coupling, permeability, energy dissipation, acoustic emission*

Introduction

With the gradual reduction of shallow resources, exploitation of deep resources had become urgent. The rock in deep strata was in complex geology with high geostress, high porewater pressure and high temperature, so the mechanical properties of the deep rock showed significant variability from that of the shallow rock [1-3].When the deep rock had disturbed by the excavation process, the in situ stress adjusted, and the stress around rocks was corresponded to change. Different stress conditions may cause the fracture opening/closing or shear expansion, which affected the formation of flow paths, the seepage characteristics of rocks would be changed [4]. So the mechanical properties of rocks under hydro mechanical coupled loads had significantly difference [5-7]. Many laboratory tests have been conducted to study the permeability evolution of rock samples including limestone, sandstone, and granite under triaxial-compression [8-11]. Shao *et al.* [12] carried out tests on brittle rocks to analyze the relationship between permeability and deviatoric stress. Ma *et al.* [13] carried out conventional triaxial tests

* Corresponding author, e-mail: youshuang@ustb.edu.cn

on sandstone to obtain the relationship between permeability and confining pressure. Yan *et al.* [14] pointed out that the permeability of rocks was positively correlated with their internal damage level. For the energy evolution in the process of stress loading, Meng *et al.* [15] obtained the energy variation tendency of rock under different stress loading rates through uniaxial cyclic loading and unloading tests of sandstone. Li *et al.* [16] calculated the ratio of dissipated energy to describe the deformation and failure mode of rock, obtained the total strain energy, elastic strain energy and dissipated strain energy of granite under different confining pressure conditions. In order to study the progressive failure characteristics of rocks, acoustic emission technology was used to characterize rock fractures at different stages by acoustic emission signal. Moradian *et al.* [17] and Jia *et al.* [18] used acoustic emission study the damage evolution of rock at various stress stages. Zhang *et al.* [19] analyzed the acoustic emission signals by fractal dimension in compression experiments.

This study aimed to study hydraulic properties and energy dissipation of deep hard rock under hydraulic-mechanics (H-M) coupling and cycling loads, the granites were taken from the deep strata (more than 1000 m). In this paper, a series of triaxial cyclic loading and unloading experiments under H-M coupling conditions were carried out. The high confining pressure and high osmotic pressure were applied to the sample to simulate the deep geostress environment, the mechanical properties and permeability of the rock during the loading and unloading process were analyzed. More importantly, rock permeability at the post-peak phase was analyzed, the influence of unloading confining pressure on the deep rocks was discussed. The results would provide a basis for the exploitation and excavation for the deep rocks.

Experimental preparation

Granite specimen and experimental methods

The rock samples used in the test are monzonitic granite in deep stratum, the depth of the samples are –1300 m to –1500 m. The average density of the sample is $2.65 \cdot 10^3$ kg/m^3, and the average porosity is about 0.5%. By component analysis, the mineral composition of granite is basically the same. Sample numbers of –1300 m, –1400 m, and –1500 m are defined as G13, G14, and G15, respectively. In order to reflect the stratum environment, the loading conditions were designed according to in-situ stress and porewater pressure from monitoring data. The confining pressure is set to 34.45, 37.10, and 39.75 MPa, respectively. The osmotic pressure is set to 13, 14, and 15 MPa, respectively. The first unloading point is set to 100 MPa, and then the unloading point is increased by 40 MPa in turn. The loading and unloading rate is set to 0.02% per minute and 0.04% per minute, respectively. After each unloading, keep the confining pressure and osmotic pressure unchanged and carry out the seepage for a period of time. After the sample failure, remove the axial deviation stress. Release the confining pressure step by step and kept the permeability constant. Measure the permeability under each confining pressure value. The loading process is shown in fig. 1. According to Darcy's law, the formula for calculating permeability can be derived as eq. (1) [20]:

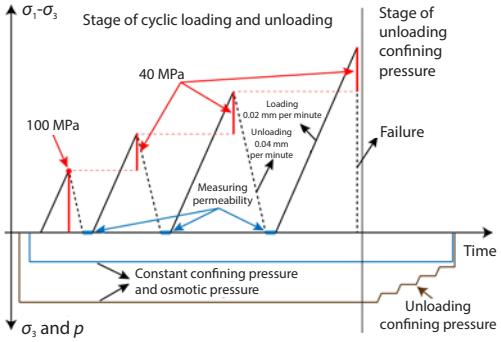

Figure 1. Experiment procedure skeleton

$$k = \frac{\mu LV}{A\Delta P\Delta t} \tag{1}$$

where k [m^2] is the permeability of rock sample, μ – the dynamic viscous coefficient of water, $\mu = 1 \cdot 10^{-3}$ Pa·s ($T = 20$ °C), L – the height of the sample, Δt – time difference, A – the cross-sectional area of the sample, and ΔP [Pa] – the osmotic pressure difference at both ends of the test sample.

Experimental results and analysis

Stress-strain relationship of deep granite under H-M coupling tests

With the increase of the axial deviating stress, the curve shows typical linear elastic characteristics at the initial stage of the experiment, fig. 2. Under the confining pressure of 34.45 MPa, 37.10 MPa, and 39.75 MPa, the peak stress of the sample reached 405.1 MPa, 417.7 MPa, and 450.9 MPa, respectively. Linearly fit the principal stress relationship of each group of rock samples, as shown in fig. 3. It can be seen that under the confining pressure of 30-40 MPa interval, the peak stress of granite increases linearly with the confining pressure, and the linear fitting coefficient is 0.94. Strength prediction can still be performed according to a linear law, which is quite different from soft rock. In the process of loading and unloading, the stress and strain have obvious hysteretic loops. The post-peak curve has typical brittleness characteristics. After reaching the peak strength, the rock sample suddenly breaks and a significant stress drop occurs.

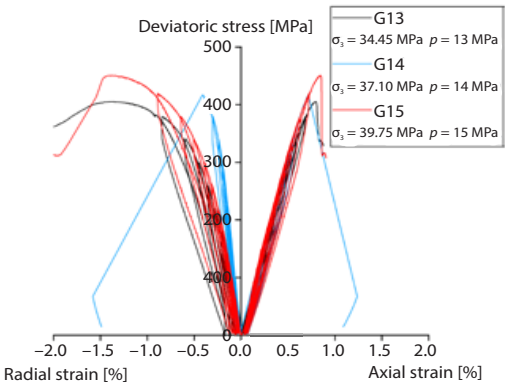

Figure 2. Results of the cyclic triaxial test under different confining pressures and seepage pressure

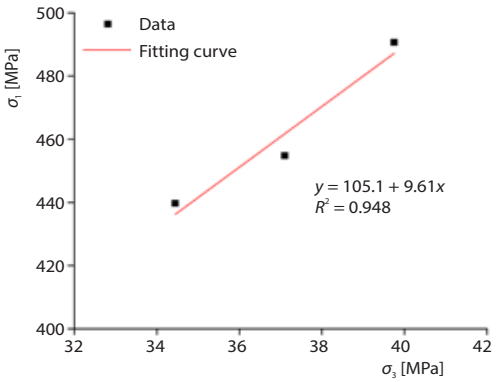

Figure 3. Relationship between principal stresses

Energy dissipation characteristics during loading process

According to the cyclic loading and unloading stress-strain curve, the ratio of the dissipated energy to the total input energy is calculated, as shown in fig. 4. In the initial stage of loading, the ratio is at a relatively high level. After 2-3 cycles, the ratio reaches a relatively low value. In the loading process, the damage of the internal structure of the rock increases gradually, and the proportion of dissipated energy begins to

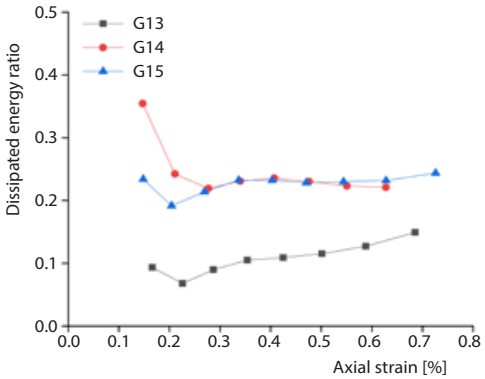

Figure 4. Dissipation energy ratio in cyclic loading and unloading

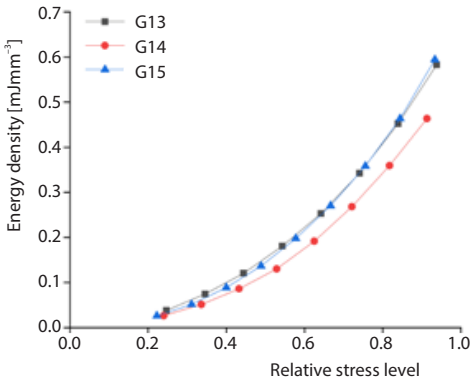

Figure 5. Relative stress level-elastic energy density curve

increase slowly. It can be seen from the figure that the overall dissipative energy of G14 and G15 is significantly higher than that of G13. According to the permeability analysis below, the internal fissures of the G14 and G15 are more developed than the G13. Therefore, in the loading and unloading cycle, a large amount of input energy is consumed due to the mechanism of mutual friction between the cracks.

The energy density of each rock sample in different cyclic loading stages is calculated, as shown in fig. 5. The curve shapes are basically the same, showing an accelerating growth trend. Generally, the larger the confining pressure of the rock, the higher the energy density. The energy density of the G15 sample is significantly higher than that of G14, and the growth rate is the fastest. However, the curve of the G13 with the lowest confining pressure is basically coincident with G15, and is still slightly higher than the G15 sample before the relative stress level reaches 0.7. It can be considered that since the internal crack of the G14 and G15 are more developed than the G13, the seepage water inside the rock significantly affects the energy storage capacity. The seepage water in the fissure reduces the friction between the rock crack surfaces. Therefore, the more the seepage channel of the rock develops, the lower its energy storage capacity.

Table 1. Permeability of each cycle of the sample

Cycles	Specimen number		
	G13	G14	G15
1	$2.4382\cdot10^{-19}$ m^2	$3.5588\cdot10^{-18}$ m^2	$1.8617\cdot10^{-18}$ m^2
2	$1.3943\cdot10^{-19}$ m^2	$3.4309\cdot10^{-18}$ m^2	$1.4914\cdot10^{-18}$ m^2
3	$8.2244\cdot10^{-20}$ m^2	$3.3005\cdot10^{-18}$ m^2	$1.2310\cdot10^{-18}$ m^2
4	$5.4702\cdot10^{-20}$ m^2	$2.9424\cdot10^{-18}$ m^2	$1.0741\cdot10^{-18}$ m^2
5	$5.4269\cdot10^{-20}$ m^2	$3.1028\cdot10^{-18}$ m^2	$2.0592\cdot10^{-18}$ m^2
6	$6.1588\cdot10^{-20}$ m^2	$2.5121\cdot10^{-18}$ m^2	$2.6963\cdot10^{-18}$ m^2
7	$7.6453\cdot10^{-20}$ m^2	$2.4311\cdot10^{-18}$ m^2	$1.9815\cdot10^{-18}$ m^2
8	$8.7417\cdot10^{-20}$ m^2	$2.7163\cdot10^{-18}$ m^2	$6.9320\cdot10^{-19}$ m^2
9	N/A	N/A	$6.4938\cdot10^{-19}$ m^2

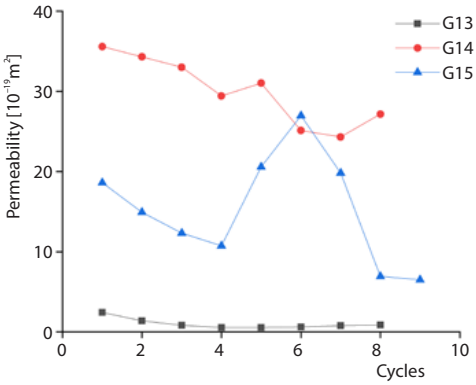

Figure 6. Relationship between permeability and number of loading and unloading cycles

Characteristics of permeability change during cyclic loading and unloading

The permeability of rock samples after each unloading stage is calculated by the eq. (1), and the results shown in tab. 1 and fig. 6. There are great differences in permeability of samples after the first cycle. Among them, the permeability of G14 was the highest, reaching $3.5588\cdot10^{-19}$ m^2. The permeability of G15 and G13 was 52.31% and 6.85% of that of G14, respectively. The difference can reach an order of magnitude. Granite is a typical low permeability rock, the permeability is mainly affected by the pore and crack morphology, showing great individual differences.

With the loading and unloading cycle proceeding, the permeability of the samples gradually decreases. The G13 reached a relatively low point at the fifth cycle, and that of G14 and G15 reached the relatively low level after the fourth cycle. At this time, the specimens reached the peak stress of 64.18%, 52.67%, and 48.79%, respectively, which indicates that the main performance of the rock is the closure of internal primary pore and crack under the deviatoric stress. The new crack is not connected with the existing seepage channel. When the axial deviatoric stress continues to be applied, the permeability of G14 increases slightly after the fifth cycle, while that of G15 increases significantly after the 5-7 cycles, even exceeds the initial permeability. It indicates that the internal cracks of the rock gradually develop, new cracks and the primary cracks begin to connect with each other. Meanwhile, the radial strain of rock increases significantly, and the volume strain exceeds the peak value. Since the rock is composed of irregular mineral particles, the two sides of the new crack are not smooth. With the increase of rock deformation, the fracture surface is slipped relatively under the influence of loading. The minerals on both sides of the seepage channel are broken due to the dislocation, blocking the seepage path and resulting in a decrease of permeability. Therefore, the permeability of the sample reaches the lowest level in the later stage of the cycle. On the whole, the permeability decreases gradually with the loading before 50% of the peak stress. The trend of monotonous change of permeability disappears when loading continues. After exceeding 50% of the peak stress, the permeability fluctuation of the sample is mainly determined by the characteristics of the seepage channel.

Permeability evolution during confining pressure unloading process

The relationship between permeability and confining pressure reduction is obtained, as shown in fig. 7. The dotted line in the figure is the permeability calculated at the last unloading before the peak stress, which is used as a benchmark to compare the changes of permeability. When the G15 was failure, a crack of 3 mm in width appeared in the rock sample, the oil quickly enters the inside of the sample, so the corresponding permeability cannot be measured.

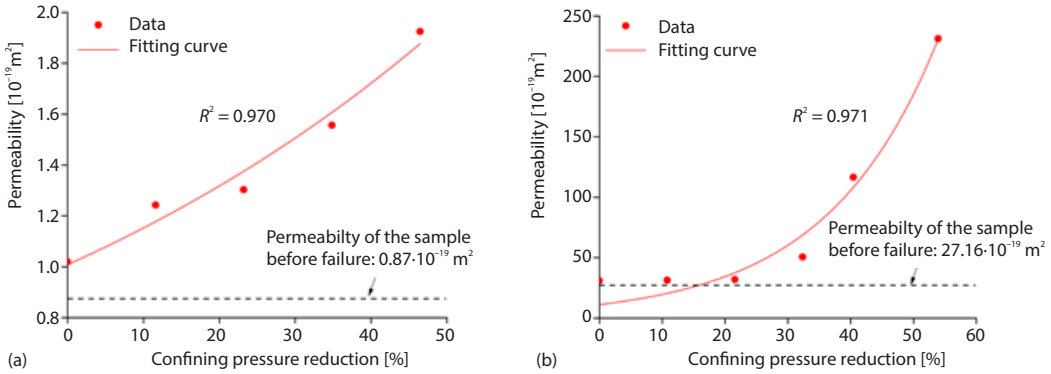

Figure 7. Relationship between permeability and confining pressure reduction; (a) the G13, (b) the G14

For the G13 specimen, the main crack does not penetrate the top and bottom of the specimen after failure, and the two main cracks extend from the top of one side to the middle of the rock side. For G14 and G15 specimens, the main crack forms a penetrating channel between the top and bottom, and the crack aperture of the G15 is obviously larger than that of

the G14. Comparing the permeability of two specimens with post-peak stage, it can be found that the permeability is higher than the permeability after the last unloading stage before the peak. The permeability of the G13 increases rapidly after failure, while that of the G14 specimen does not increase significantly at the initial stage of confining pressure unloading. After confining pressure decreases more than 30%, the permeability begins to increase rapidly. The permeability of G13 increased to 188.73% when confining pressure was reduced to 46.44%, and that of G14 increased to 746.77% when confining pressure was reduced to 53.91%. There was still a difference of 1-2 orders of magnitude between the permeability of the two groups of specimens. By exponential fitting of the data points of the samples, the permeability has a good exponential relationship with the reduction level of confining pressure, and the fitting coefficients are above 9.70. For rock mass with through crack, it is more sensitive to the influence of confining pressure reduction. This is mainly because under the action of high water pressure, water can easily flow along the seepage channel. When there is no through crack in the specimen, the seepage water will be restricted by higher confining pressure after reaching the side of the specimen, resulting in stagnation of seepage. Considering the protection experimental system, the confining pressure is always higher than the applied osmotic pressure, but from the shape of the fitting curve, it can be predicted that if the confining pressure is further reduced, the permeability of the sample will increase faster. Therefore, for water-rich strata, the reduction of rock stress caused by excavation of rock engineering may lead to the rapid outflow of ground water. Especially considering that blasting and excavation will lead to an increase in rock mass cracks, the increase in permeability will be more significant.

Granite failure characteristics by acoustic emission monitoring

The acoustic emission signals of the sample during cyclic loading and unloading are recorded by the acoustic emission detecting device. Due to the limited space, the G13 is taken as an example, as shown in fig. 8. It can be seen from the figure that only a small amount of acoustic emission signals appear near the unloading point during the first three cycles, and the overall magnitude is small, the cumulative curve grows slowly. When the fourth cycle unloading point is reached, the ringing count increases sharply and the cumulative curve increases rapidly. In each subsequent cycle, a large number of acoustic emission occurred, and the cumulative curve showed a step-like increase, which was basically consistent with the acoustic emission signal characteristics of the triaxial cyclic loading and unloading experiment without seepage. As shown in fig. 8, the acoustic emission signal only appears in the loading stage in the first 5 cycles. The acoustic emission signal also appeared during the 6-8th unloading process. In the sixth unloading stage, the acoustic emission signal value is small and very concentrated, and the value becomes large in the seventh unloading stage. In the eighth unloading phase, the acoustic emission signal began to appear densely. This indicates that under the action of high osmotic pressure, as the number of rock cracks increases, the higher pore water pressure also causes cracking of the rock. During the unloading stage, the axial deviator stress gradually decreases, and the high-pressure seepage water enters the sample lead to an increase in the pore water pressure, and a stress concentration is formed at the crack tip. This process caused an increase in the crack and an acoustic emission signal.

Figure 9 shows the acoustic emission ringing counts for the G13 during the unloading confining pressure stage. It can be seen from the figure that each time the 4 MPa confining pressure was unloaded, a certain number of ringing counts appear, and the appearance of the acoustic emission signal has obvious stage characteristics. At the beginning of the confining pressure

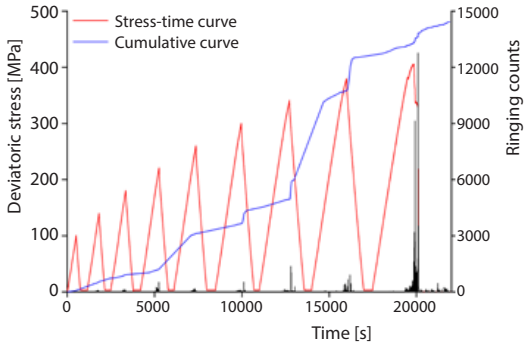

Figure 8. Results of AE monitoring tests

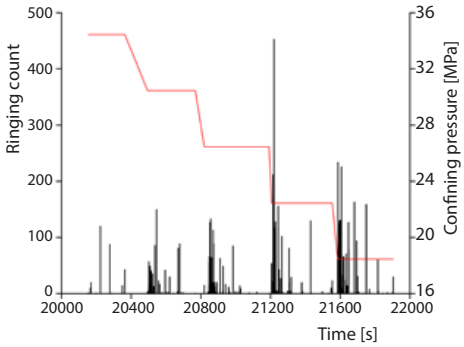

Figure 9. Relationship of confining pressure and ringing count

unloading, the amount of acoustic emission signals is small. When the confining pressure of the G13 was reduced to 20.45 MPa, a large number of ringing counts appeared. Therefore, for samples with existing cracks, under the action of high osmotic pressure, when the confining pressure is reduced by more than 30%, special attention should be paid to the damage of the seepage water to the rock.

Conclusion

The stress-strain curve of the deep strata granite exhibits typical brittle characteristics under the 34-40 MPa confining pressure and 13-15 MPa pore water pressure. The initial permeability of the sample is related to the internal crack characteristics. With the increase of loading and unloading cycle test times, the permeability generally shows a downward trend before rock failure. After the sample failure, the permeability shows an exponential growth with the decrease of the confining pressure. The permeability of the sample without the through crack is much lower than that of the sample with the through crack. The porewater pressure seriously influences the fractures developing in rocks, the energy storage capacity and the dissipative energy of granite decreased obviously as the seepage increased under the high osmotic pressure. As the fracture continues to develop, energy dissipation will cause the acoustic emission signal released. After reaching the peak stress, the rock sample suddenly breaks with a large number of acoustic emission signals.

Acknowledgment

This work was financially supported by the State Key Research Development Program of China (Grant No. 2016YFC0600801), and National Natural Science Foundation of China (Grant No. 51774021).

Nomenclature

A – cross-sectional area of the test sample, [m^2]
k – permeability of rock sample, [m^2]
L – height of the sample, [m]
ΔP – osmotic pressure difference, [Pa]
Δt – time difference, [s]
V – volume of seepage fluid, [m^3]

Greek symbol

μ – dynamic viscous coefficient of water, [Pa·s]

Acronym

H-M – hydraulic-mechanics

References

[1] Qian, Q., *et al*., Effects of the Axial in Situ Stresses on the Zonal Disintegration Phenomenon in the Surrounding Rock Masses Around a Deep Circular Tunnel, *Journal of Mining Science*, *48* (2012), 2, pp. 276-285
[2] Zhou, X. P., *et al*., Excavation-Induced Zonal Disintegration of the Surrounding Rock Around a Deep Circular Tunnel Considering Unloading Effect, *International Journal of Rock Mechanics and Mining Sciences*, *64* (2013), Dec., pp. 246-257
[3] Zhou, H., *et al*., Analysis of Mechanical Behavior of Soft Rocks and Stability Control in Deep Tunnels, *Journal of Rock Mechanics and Geotechnical Engineering*, *6* (2014), 3, pp. 219-226
[4] Cheng, C., *et al*., Failure Behavior of Granite Affected by Confinement and Water Pressure and Its Influence on the Seepage Behavior by Laboratory Experiments, *Materials*, *10* (2017), 7, 798
[5] Ji, S. H., *et al*., Influence of Pressure Change During Hydraulic Tests on Fracture Aperture, *Ground-Water*, *51* (2013), 2, pp. 298-304
[6] Rutqvist, J., *et al*., The Role of Hydro Mechanical Coupling in Fractured Rock Engineering, *Hydrogeology Journal*, *11* (2003), 1, pp. 7-40
[7] Gao, M. Z., *et al*., Field Experiments on Fracture Evolution and Correlations Between Connectivity and Abutment Pressure under Top Coal Caving Conditions, *International Journal of Rock Mechanics and Mining Science*, *111* (2018), Nov., pp. 84-93
[8] Brace, W. F., *et al*., Permeability of Granite Under High Pressure, *Journal of Geophysical Research*, *73* (1968), 6, pp. 2225-2236
[9] Li, S. P., *et al*., Effect of Confining Pressure, Pore Pressure and Specimen Dimension on Permeability of Yinzhuang Sandstone, *International Journal of Rock Mechanics and Mining Science* and *Geo Mechanics Abstracts*, *34* (1997), 3, pp. 432-432
[10] Wang, J. A., *et al*., Fluid Permeability of Sedimentary Rocks in a Complete Stress-strain Process, *Engineering Geology*, *63* (2002), 3, pp. 291-300
[11] Wang, H. L., *et al*., Anisotropic Permeability Evolution Model of Rock in the Process of Deformation and Failure, *Journal of Hydrodynamics*, *24* (2012), 1, pp. 25-31
[12] Shao, J. F., *et al*., Coupling between Anisotropic Damage and Permeability Variation in Brittle Rocks, *International Journal for Numerical and Analytical Methods in Geo Mechanics*, *29* (2005), 12, pp. 1231-1247
[13] Ma, D., *et al*., Experimental Investigation of Seepage Properties of Fractured Rocks under Different Confining Pressures, *Rock Mechanics and Rock Engineering*, *46* (2013), 5, pp. 1135-1144
[14] Yan, C. L., *et al*., Permeability Change Caused by Stress Damage of Gas Shale, *Energies*, *10* (2017), 9, 1350
[15] Meng, Q. B., *et al*., Effects of Acoustic Emission and Energy Evolution of Rock Specimens under the Uniaxial Cyclic Loading and Unloading Compression, *Rock Mechanics and Rock Engineering*, *49* (2016), 10, pp. 3873-3886
[16] Li, D., *et al.*, Energy Evolution Characteristics of Hard Rock during Triaxial Failure with Different Loading and Unloading Paths, *Engineering Geology*, *228* (2017), Oct., pp. 270-281
[17] Moradian, Z. A., *et al*., Evaluating Damage during Shear Tests of Rock Joints Using Acoustic Emissions, *International Journal of Rock Mechanics and Mining Sciences*, *47* (2010), 4, pp. 590-598
[18] Jia, L., *et al*., Experimental Study and Numerical Modelling of Brittle Fracture of Carbonate Rock under Uniaxial Compression, *Mechanics Research Communications*, *50* (2013), June, pp. 58-62
[19] Zhang, R., *et al*., Fractal Analysis of Acoustic Emission during Uniaxial and Triaxial Loading of Rock, *International Journal of Rock Mechanics and Mining Sciences*, *79* (2015), Oct., pp. 241-249
[20] Heiland, J., Laboratory Testing of Coupled Hydro-Mechanical Processes During Rock Deformation, *Hydrogeology Journal*, *11* (2003), 1, pp. 122-141

Paper submitted: July 2, 2018
Paper revised: November 13, 2018
Paper accepted: December 24, 2018